

Paleomagnetism of the Middle Jurassic Sedimentary Rocks of the Elgon Formation of the Ulban Terrane

A. Yu. Peskov^{a,*}, A. V. Kudymov^a, S. V. Zybrev^a, A. S. Karetnikov^a, M. V. Arkhipov^a,
A. I. Tikhomirova^a, and A. N. Didenko^a

^a Kosygin Institute of Tectonics and Geophysics, Far East Branch, Russian Academy of Sciences,
ul. Kim Yu Chena 65, Khabarovsk, 680000 Russia

*e-mail: itig@itig.as.khb.ru

Received March 19, 2020; revised November 27, 2020; accepted January 22, 2021

Abstract—The paper presents the first findings of paleomagnetic studies on Middle Jurassic sedimentary rocks of the Elgon Formation of the Ulban Terrane from the coastal outcrops along the Ulban Bay (53.5° N, 137.7° E). Demagnetization yielded a ChRM component of the pre-folding age. No inclination shallowing effect for the ChRM vector was revealed in sandstone specimens of the Elgon Formation. The paleomagnetic pole coordinates and the paleolatitude at which the studied rocks deposited were calculated: Plat = −34.3 (34.3)°; Plong = 161.2 (341.2)°; dm = 2.7, dp = 5.3, paleolatitude = 0.1° (+2.7°/−2.6°) S. The acquired paleomagnetic data are evidence of the deposition of the rocks of the Ulban Terrane in the Middle Jurassic at the boundary between the Asian paleocontinent and the Paleo-Pacific, which later formed part of the Sikhote Alin Orogenic Belt.

Keywords: paleomagnetism, paleolatitude, magnetization, inclination shallowing, Ulban Terrane, Sikhote Alin Orogenic Belt, Mongol–Okhotsk Orogenic Belt

DOI: 10.1134/S1819714021030052

INTRODUCTION

The Ulban Terrane, or the neacontinental turbidite basin, is located on the western coast of the Sea of Okhotsk and is adjacent to the northern termination of the Sikhote Alin Range. It has a sublatitudinal extent and an arcuate wedge-like shape and is approximately 160 km wide and 400 km long. The terrane is composed of thick (more than 11 km) series of terrigenous fragmentary rock deposits, which are dominantly sandstones with subordinate siltstones and argillites with rare layers of conglomerates, gravelites, and sedimentary breccias. Cherts and basalts are known to have been found among terrigenous deposits [3–7]. The deposits are crumpled into a system of the E- and NW-striking folds and build up the tectonic plates of the southern vergence [3–8, 22]. The Ulban Terrane is interpreted as a fragment of the Early Mesozoic accretionary prism that is mainly composed of turbidites [3, 22]. In the north, the terrane borders with the Paleozoic accretionary complexes of the Mongol–Okhotsk Orogenic Belt (MOOB), whereas in the east it is bounded by the Mesozoic accretionary complexes of the Sikhote Alin Orogenic Belt (SAOB). The papers that deal with the primary original materials on the rocks of the Ulban turbidite basin and their analysis are not numerous [4, 19, and others]; moreover, their number is insufficient, given that they were published

more than 40 years ago. Its tectonic position falls within the junction area of these two orogenic belts and the general strikes of the inner structure are concordant with the strikes of the adjacent orogenic belt structures. This makes our understanding of tectonic belonging of the Ulban Terrane either to the MOOB or to the SAOB rather vague.

It is generally accepted that the Ulban Terrane is considered as part of the structure of the eastern segment of the MOOB [3, 18, 22, 24, and others]. Such understanding of its tectonic position originated from the concepts proposed by Nagibina [21] on the tectonic zonation of the Mongol–Okhotsk Belt, whose eastern (locking) element is the Tugor–Nimelensky Synclinorium comprising the Ulban, Mevachan and Omel'da zones [21, p. 13].

A very different conception of the tectonic position of the Ulban Terrane was postulated by V.V. Golozubov, who assumed that the “...modern configuration and the inner structure of the Ulban Terrane resulted from heaping that occurred in front of the block-impendents (these are likely northward located paleozooids of the Galam segment of the Mongol–Okhotsk Belt); a considerable (if not the dominant) part of the Ulban turbidite basin was located southward of its present day location along the eastern edge of the Bureya Massif. Hence, it seems unlikely to be justifi-

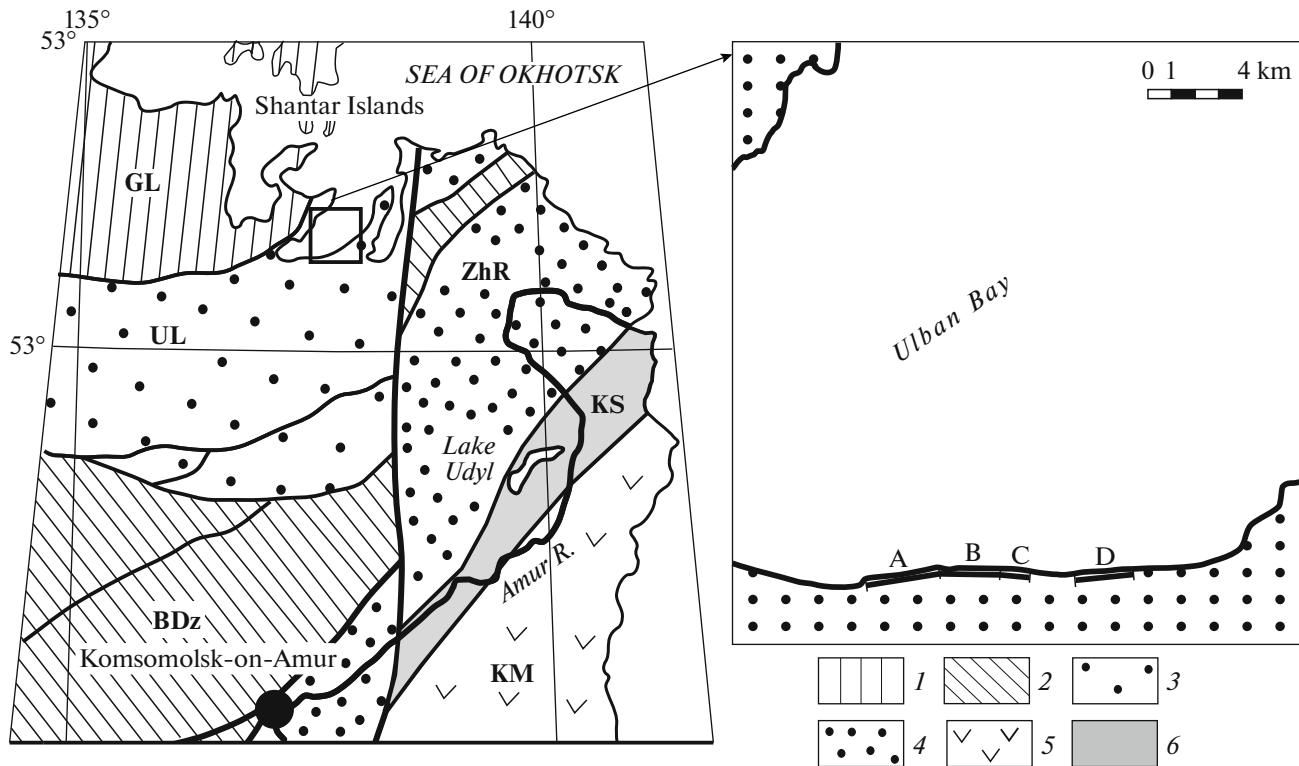


Fig. 1. A scheme showing the locations of the constructed geological sections (A, B, C, and D fragments) (see Figs. 2 and 3). (1) Paleozoic Galam (GL) Terrane; (2–6) terranes-fragments: (2) Jurassic accretionary prisms (BDz, Badzhal); (3) Jurassic nearcontinental turbidite basin (UL, Ulban); (4) Cretaceous syn-strike-slip turbidite nearcontinental basin (ZhR, Zhuravlevka–Amur Terrane); (5) Hauterivian–Albian island-arc system of the Kema Terrane (KM); (6) Hauterivian–Albian accretionary prism (KS, Kiselevka–Manoma). Tectonic scheme is given after [3].

able to include the Ulban Terrane in the Mongol–Okhotiya structures due to the fact that this terrane laterally replaces the terranes of the Jurassic accretionary prisms of the eastern frame of Eurasia” [7, p. 54].

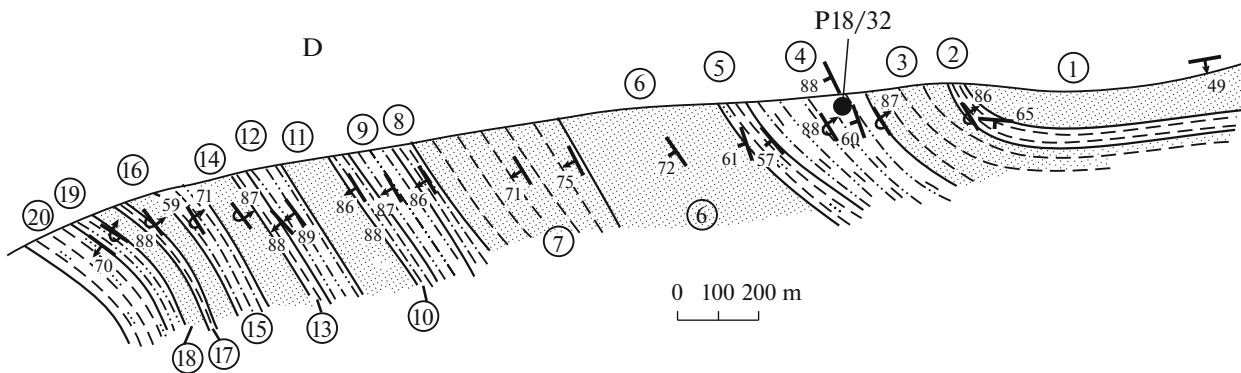
In this paper, we attempt to present the results of paleomagnetic studies on Middle Jurassic fragmentary rock deposits of the Elgon Formation of the Ulban Terrane. The main goal of our study was to determine the paleolatitudes at which these rocks were deposited on the assumption that this paleogeographic information would sufficiently contribute to a validated interpretation of the tectonic position of the Ulban Ter-

rane, and could help clarify the belonging of the Ulban Terrane to the MOOB or to the SAOB.

THE GEOLOGICAL CHARACTERISTIC OF THE STUDY REGION

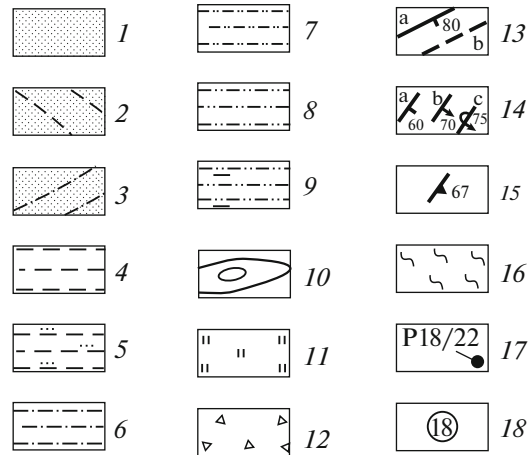
The geological data on the Ulban Terrane were mainly derived from the geological surveys on a scale of 1 : 200000 performed in the late 1960s [4, 5, 19, and others]. The stratigraphic concepts developed on the terrane deposits at that time [2, 16, 17] have not significantly changed thus far. Since then, no new publications dealing with the original data on their structure

Fig. 2. The schematic geological section (plan) of the Middle Jurassic coastal deposits (D fragment) along the Ulban Bay, and the attached stratigraphic column: (1) fine-grained and fine-to-medium grained sandstones, in some cases with rare thin siltstone interbeds; (2) fine-grained and fine-to-medium grained sandstones with rare siltstone beds; (3) fine-grained and fine-to-medium grained sandstones with rare siltstone members (0.3–1.5 m), containing thin fine-grained sandstone interbeds; (4) massive, more rarely thin-bedded siltstones, in some cases with thin (up to 5 cm) fine-grained sandstone interbeds; (5) siltstones with rare fine-grained sandstone beds; (6) equal-ratio fine-grained sandstone and siltstone alternation; (7) alternated fine-grained sandstones and siltstones with dominant sandstones; (8) alternated fine-grained sandstones and siltstones with strongly dominant sandstones; (9) alternated fine-grained sandstones and siltstones with strongly dominant sandstones with rare siltstone beds; (10) lens-shaped conglomerate interbeds; (11) siliceous rocks alternated by silica-clayey ones; (12) rubble–block talus; (13) faults: a, ascertained, with dips shown, b, supposed; (14) strikes and dips of lamination, with dips shown: (a) with non-determined “top-bottom” polarity, (b, c) with determined “top-bottom” polarity (b) normal, (c) overturned); (15) schistosity strikes and dips, with dips shown; (16) schistosity zone; (17) sampling sites of the oriented samples collected for paleomagnetic studies, and their numbers; (18) numbers of members.



Stratigraphic column

System	Section	Formation	Bed no.	Thickn.
Jurassic	Middle	Elgon	20	75
			19	35
			18	35
			17	10
			16	32
			15	52
			14	60
			13	25
			12	45
			11	80
			10	35
			9	70
			8	30
			7	225
			6	228
			5	34
			4	112
			3	130
			2	32
			1	63



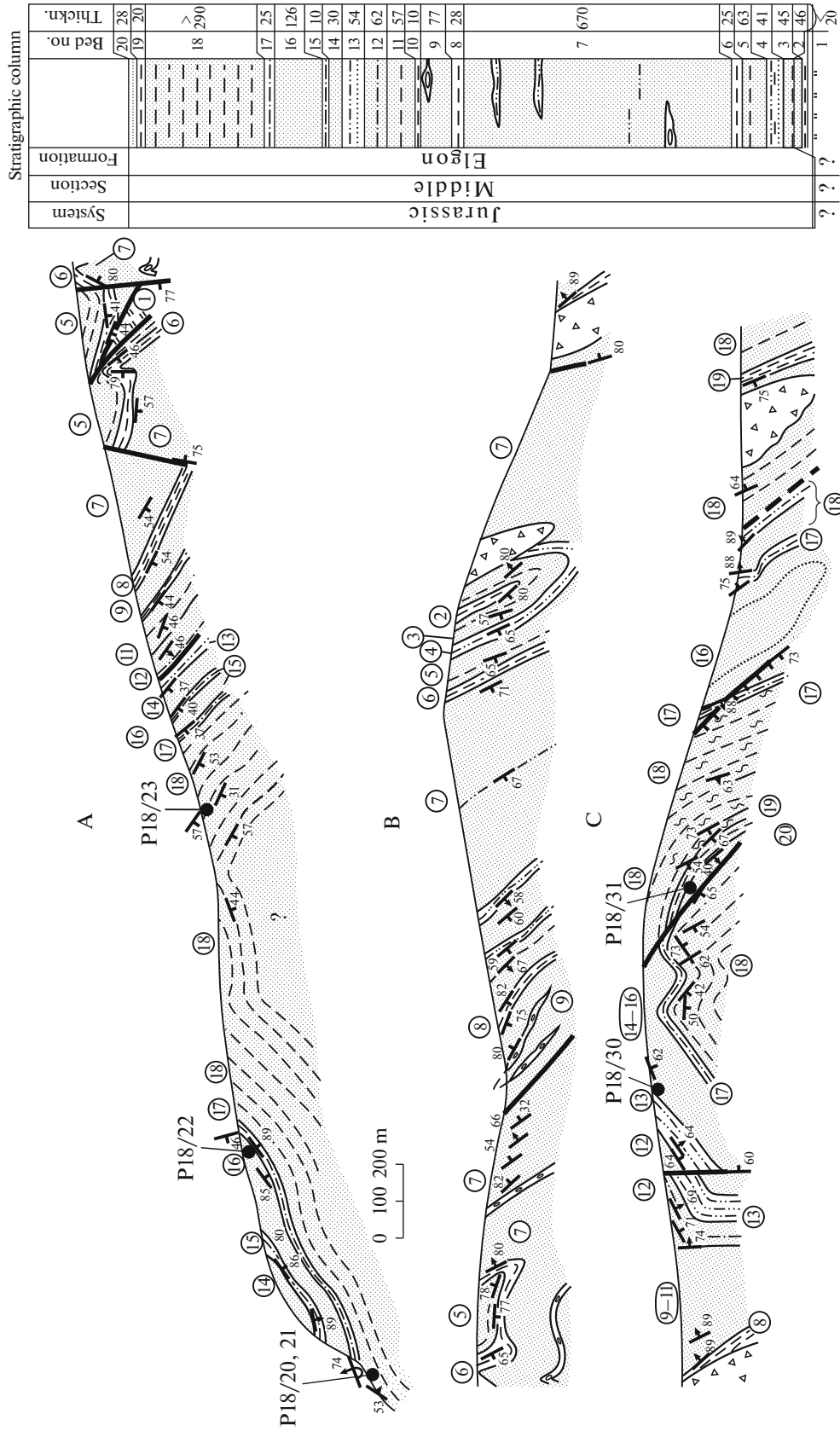


Fig. 3. The sections of Middle Jurassic coastal deposits (A, B, and C fragments) along the Ulban Bay and the summary stratigraphic column. For explanations see Fig. 2.

have appeared due to poor accessibility of the explicitly manifested coastal outcrops of the rocks deposited along the Ulban Bay.

Primarily, the coastal deposits studied along the Ulban Bay (Figs. 1–3) have been assigned to the upper Lower Jurassic owing to their being concordantly overlain by the deposits that contained the Middle Jurassic, Aalenian–Bajocian fauna [4, 5]. Combined with the overlying deposits, these deposits were later considered as part of the Elgon Formation [9].

A detailed study of the section of the Elgon Formation along the coast of the Ulban Bay (Figs. 1–3) has shown that it is mainly composed of the thick sandstone beds, and, to a lesser degree, the members with alternated siltstones and sandstones, and siltstone beds and rare lens-shaped conglomerates. The fragment of siliceous and silica-clayey deposits is present in tectonic constraints (Fig. 3a).

The section studies have revealed the massive and laminated varieties of fine- and medium-grained sandstones composing 45 to 670-m thick members that contain rare siltstone layers (from a few centimeters to a few kilometers thick) and rare siltstone members (0.3–1.5 m thick) with thin fine-grained sandstone interbeds.

The deposits were subdivided into the following members: (1) those with equal sandstone-to-siltstone ratios; (2) those with dominant sandstones; and (3) those with strongly dominant sandstones. The members where the sandstone-to-siltstone ratios are equal are made up of fine-grained sandstones and siltstones whose thicknesses range from 0.5 to 30 cm, and from 0.3 to 30 cm, respectively. In some cases, these members contain sandstone beds up to 2-m thick. The alternated members with dominant sandstones are built up of up to 30-cm thick fine-grained sandstones and siltstone layers a few centimeters thick. The members where sandstones are strongly dominant are composed of fine-grained sandstones with the thicknesses varying from 5 cm to a few meters and siltstones with thicknesses of up to a few centimeters. In the studied section, these members are prevalent. In some cases, they contain siltstone beds with fine-grained sandstone interbedding.

Separate siltstone beds are 10 to 34 m thick and contain sandstone interbeds up to a few cm thick.

Conglomerate beds with variable thicknesses (up to 10 m) contain sandstone and siltstone pebble (0.5–40 cm) of different degrees of roundness, which is distributed in the medium-grained sandstone matrix (20–40%). The pebble sandstones are fine-grained massive, fine-grained laminated, and medium-to-coarse grained massive with siltstone fragments.

The studied deposits show the indications of turbidites. They are the most pronounced in the members with rhythmical sandstone and siltstone alternation where these rocks exhibit equal ratios. The rhythms are characterized by an erosional lower boundary,

which bears wash-up traces and show the presence of outliers of the underlying siltstones. The sandy part of the rhythms displays a pronounced gradational assortment with more coarse-grained material at their bottoms. Casts of the current streams, flute casts, and traces of traction are observed at the rhythm bottoms [10]. In rare cases, sedimentary textures of the Boum sequence are identifiable. In many cases, the thick sandstone layers of the sections appear to be composite and the *A* and *AB* elements of the Boum texture sequence are recognized in some cases. Groups of fine-grained sandstone laminas and thin (up to 5 cm) fine-grained sandstone layers with thin parallel lamination are frequently found among siltstones. Such layers are interpreted as bottom flow deposits.

The Middle Jurassic sandstones have a polymictic and quartz-feldspar composition [4]; the fragmentary material accounts for 85–95% of the bulk of the rock. The fragmentary mineral grains are presented by quartz and feldspars (plagioclase and more rarely K-feldspars) with an admixture (10–30%) of fragments of siltstones, clayey, silica-clayey and siliceous rocks, and quartzites, andesites, biotite and muscovite leaflets, and pyroxene, epidote, sphene, granite, tourmaline and zircon grains, which are few in number. Cement is only observed in small-scale pores; it has a hydromicaceous-quartz and quartz-hydromicaceous composition with constant admixture of chlorite.

Siltstones are dark-gray and black. They appear to be a clayey hydromicaceous chloritized mass which accommodates the ore “dust” and siltstone clastics (exceeding 50% of the rock bulk) of quartz and feldspars [4].

The Ulban Terrane fragment studied has an irregular structure, which displays a combination of large isoclinal folds with more open and box folds. The fold limbs compose the extended (up to 3 km) segments of the section where a unilateral dipping of lamination from 37° to 89° is observed (Figs. 2 and 3). The subvertical dips are alternated by the overturned ones that do not indicate the “top–bottom” change of polarity (Fig. 2). The imbricated sheet–thrust structure of the terrane proposed by Natal'in [22] is displayed by a small-scale tectonic wedge (20 m thick) composed of siliceous and siliceous-clayey oceanic deposits, which is squeezed between sandstones (Fig. 3).

According to [22], the imbricated sheet–thrust structure of the terrane originated during the subduction stage, but the age of the deformations and their development in space and time still remain to be unclear. The Late Jurassic age of the youngest deposits and the lack of Cretaceous deposits in the structure of the Ulban Terrane may indicate that it originated at the Jurassic–Cretaceous boundary.

Table 1. The results of the paleomagnetic studies

Site	φ , °	λ , °	N_1	N_2	Bed, °		Dec _g , °	Inc _g , °	K	a_{95} , °	Dec _s , °	Inc _s , °
P18/20	53.55	137.70	8	6	337	74*	340.2	78.2	21.2	14.9	156.3	-4.3
P18/22	53.55	137.71	10	8	255	46	207.5	81.1	6.3	23.9	158.4	0.1
P18/23	53.55	137.73	10	9	215	57	162.7	58.9	14.5	14.0	190.4	11.7
P18/30	53.56	137.80	10	9	158	62	166.9	65.6	19.4	12.0	161.7	3.8
P18/31	53.56	137.81	12	8	242	54	171.1	28.6	20.6	12.5	185.9	2.8
P18/32	53.57	137.85	8	6	244	88	192.2	32.9	24.2	13.9	194.4	-30.0
P18/37	53.59	137.97	12	6	40	60*	72.7	43.1	9.1	23.5	202.2	19.8
P18/20a	53.55	137.70	8	7	337	74*	357.4	81.1	29.5	11.3	153.9	-7.6
P18/21a	53.55	137.70	7	6	337	74*	75.4	76.4	23.9	14.0	142.9	-17.5
P18/22a	53.55	137.71	10	9	255	46	131.9	81.0	14.5	14.0	148.0	-3.5
P18/23a	53.55	137.73	10	10	215	57	183.4	57.2	38.3	7.9	198.4	4.0
P18/25a	53.61	137.99	9	9	44	35	162.8	-20.2	9.1	18.0	168.6	-1.3
P18/30a	53.56	137.80	10	4	158	62	197.8	70.2	22.7	19.7	170.8	12.2
P18/31a	53.56	137.81	12	3	242	54	163.0	22.4	45.9	18.4	176.3	4.7
P18/32a	53.57	137.85	8	6	244	88	154.7	50.0	18.5	16.0	204.0	1.0
ChRM mean direction for samples ($N = 106$)							163.1	62.2	4.5	7.3		
									7.7	5.3	173.9	-0.2
ChRM mean direction for sites ($N = 15$)							161.8	62.5	5.3	18.3		
									12.0	11.5	173.9	-0.2
Paleomagnetic pole coordinates							Plat = -34.3 (34.3)°; Plong = 161.2 (341.2)°; dm = 2.7, dp = 5.3					
Paleolatitude							-0.1° (+2.7°/-2.6°)					

φ , λ , coordinates (latitude and longitude) of the sampling site; N_1 , the number of samples at the site; N_2 , the number of samples with identified ChRM; Dec, Inc, the ChRM declination and inclination in the geographical (g) and stratigraphic (s) coordinate systems; K, grouping of the ChRM distribution; a_{95} , 95% confidence oval of the ChRM; Plat, Plong, latitude and longitude of the paleomagnetic pole; dp, dm—semi-axes of the 95% confidence oval of the paleomagnetic pole; *, overridden bed. Paleomagnetic pole coordinates were determined accounting for the magnetic declination value in the sampling area, 13° W.

PETRO- AND PALEOMAGNETIC STUDIES

Investigation Technique

Petro- and paleomagnetic measurements were performed at the Khabarovsk Innovation and Analytical Center, Kosygin Institute of Tectonics and Geophysics, Far East Branch, Russian Academy of Sciences (ITiG FEB RAS) using high-precision measurement equipment (SQUID-magnetometer manufactured by 2G Enterprises, JR-6A spin-magnetometer, and the MFK-IFA Kappa-bridge) by employing modern measurement techniques [20, 26, 28].

A total of over 100 oriented sandstone samples were collected from nine sampling sites on the coastal outcrops along the Ulban Bay. Of these, six sites are spaced at 250–1600 m distances from one another over an entire section of 1727-m thick deposits (Figs. 2 and 3). One sampling site is located in the middle part of another 1408-m thick section east of the first one (Figs. 1 and 3). The other two sites are spaced at 8–10-km distances northeast of the segment *D* of the section described (see Table 1). The number of the samples was 14 to 25 at each sampling site.

The samples collected at each sampling site were divided into two equal groups: one group of samples was subjected to an alternating magnetic field (*H*-demagnetization), whereas the other group was prepared for thermal demagnetization (*T*-demagnetization). To perform paleomagnetic measurements, the samples were preliminarily cut into two cubic specimens with a 2-cm side dimensions using an electric saw equipped with a diamond disk, and 2–3 cubic specimens with a 1-cm side dimensions were prepared for petromagnetic measurements.

As mentioned above, sample demagnetization was carried out involving two techniques, namely, the temperature, and alternating magnetic field. We assume that convergence of the directions of the revealed natural remanent magnetization (NRM) components inferred from different demagnetization techniques may serve as an additional criterion for validation of the primary origin of the distinguished characteristic remanent magnetization (ChRM) component. During thermal demagnetization, the NRM was measured on a JR-6A spin-magnetometer, whereas the SQUID-magnetometer manufactured by 2G

Enterprises was employed for demagnetization by an alternating field. In order to bring the specimens from the electric oven, which is isolated by permalloy screens, to the measurement equipment, they were placed in a μ -metal container. As a rule, all specimens were demagnetized by stepwise heating up to 550–580°C temperatures and a stepwise effect of alternating field of 50–80 mT intensity. The number of demagnetization steps was dependent on the behavior of the NRM vector during demagnetization, and, as a rule, was not less than 12. The NRM components were identified using the component analysis technique and applying the PMGSC (Version 4.2) software created by Enkin [32], and illustrated by plotting the Zijderveld orthogonal demagnetization diagrams [41].

Petromagnetic studies have determined the initial magnetic susceptibility value (k_m), by using the MFK-IFA Kappa-bridge, and calculated the Königsberger ratio (Q). To estimate the probable value of the ChRM inclination shallowing for the sedimentary rocks due to compaction, we employed (1) the dependence between the anisotropy value of the initial magnetic susceptibility and the tangent of the ChRM inclination angle [31] and (2) the “Elongation–inclination” method [38, 39]. All studied specimens show a Königsberger ratio value less than 1.

The fold test, as implemented in the PMGSC (Version 4.2) software developed by Enkin [32], was used in our studies.

Investigation Results

The initial magnetic susceptibility and the NRM values of the samples studied do not show strong variations, only an order of magnitude (Fig. 4). For all samples, the Königsberger ratio values are less than 1, which is typical of the sedimentary rocks with directional (DRM) and post-directional (PDRM) origin of magnetization.

Laboratory paleomagnetic studies have analyzed a total of 144 samples that were collected from nine sampling sites with different strike and dip angles (Table 1, Figs. 2 and 3). The analysis of the results obtained involved 106 samples, in which a stable paleomagnetic signal was detected (Table 1).

The investigation results show that the NRM values obtained for the samples show a two-component composition in 90% of cases, whereas a three-component composition occurs within the remaining 10%.

As an example, Fig. 5 illustrates the results of H - and T -demagnetizations showing the two- and three-component NRM compositions.

The thermal demagnetization determined the three-component NRM composition in the P183102 sample (Fig. 5a): a low-temperature (LT) component of the NRM was revealed in the temperatures between 20–300°C, not via the starting coordinate point; a medium-temperature (MT) component was inferred

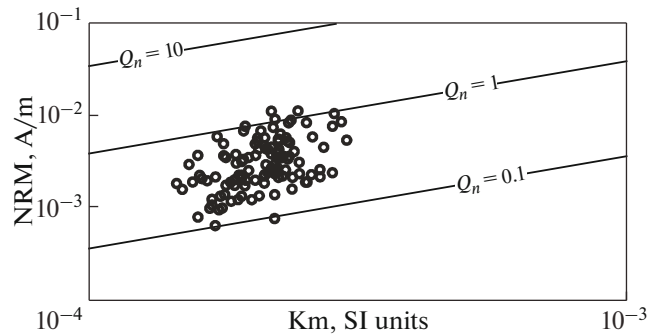


Fig. 4. A bilogarithmic diagram showing the NRM–km dependence for the studied samples.

in the temperature range from 300 to 450°C that exhibited similar behavior, and a high-temperature (HT) component of the NRM for the sample, which was determined in the temperatures from 450 to 550°C that ran via the starting coordinate point.

From the results of H -demagnetization, a three-component NRM composition has been recognized in the P182307a sample (Fig. 5b). The orthogonal demagnetization diagram clearly shows the low- (LC), medium- (MC), and high-coercitive (HC) components of the NRM in the ranges of 0–12, 12–30, and 30–48 mT, respectively. Unlike the LC and MC components, the HC component runs via the starting coordinate point.

Figures 5c and 5d illustrate the examples of a two-component NRM composition, where the LT and HT components were revealed in the case of T -demagnetization (Fig. 5c), and the LC and HC components were identified in the case of H -demagnetization (Fig. 5d). These components show behavior similar to that typical of the above-described samples with a three-component NRM composition.

We further analyzed the mean directions of the NRM components for all samples and sampling sites. A considerable site-to-site scatter in the distributions of the LT and LC components of the NRM has been observed: the confidence oval (a_{95}) ranging from 17° to 40° and the grouping of the distribution (K) varying from 5 to 16. According to their locations on the stereograms, they may be subdivided into two groups: (1) the components located in the first quadrant with the site-mean direction— $D_g = 44.6^\circ$, $I_g = 61.6$, $K_g = 44.4$, $a_{95g} = 9.2^\circ$; (2) the components located in the third and fourth quadrants with the site-mean direction— $D_g = 170.3^\circ$, $I_g = 45.4$, $K_g = 29.7$ and $a_{95g} = 11.3^\circ$. These are post-folding directions, which is shown by an increase in the grouping of their distributions by factors of 7.5 and 1.1 in the petrographic coordinate system for the first and second groups, respectively. The site-mean direction for the first group is close to, but is not coincidental with, the direction of the present day magnetic field observed in the sam-

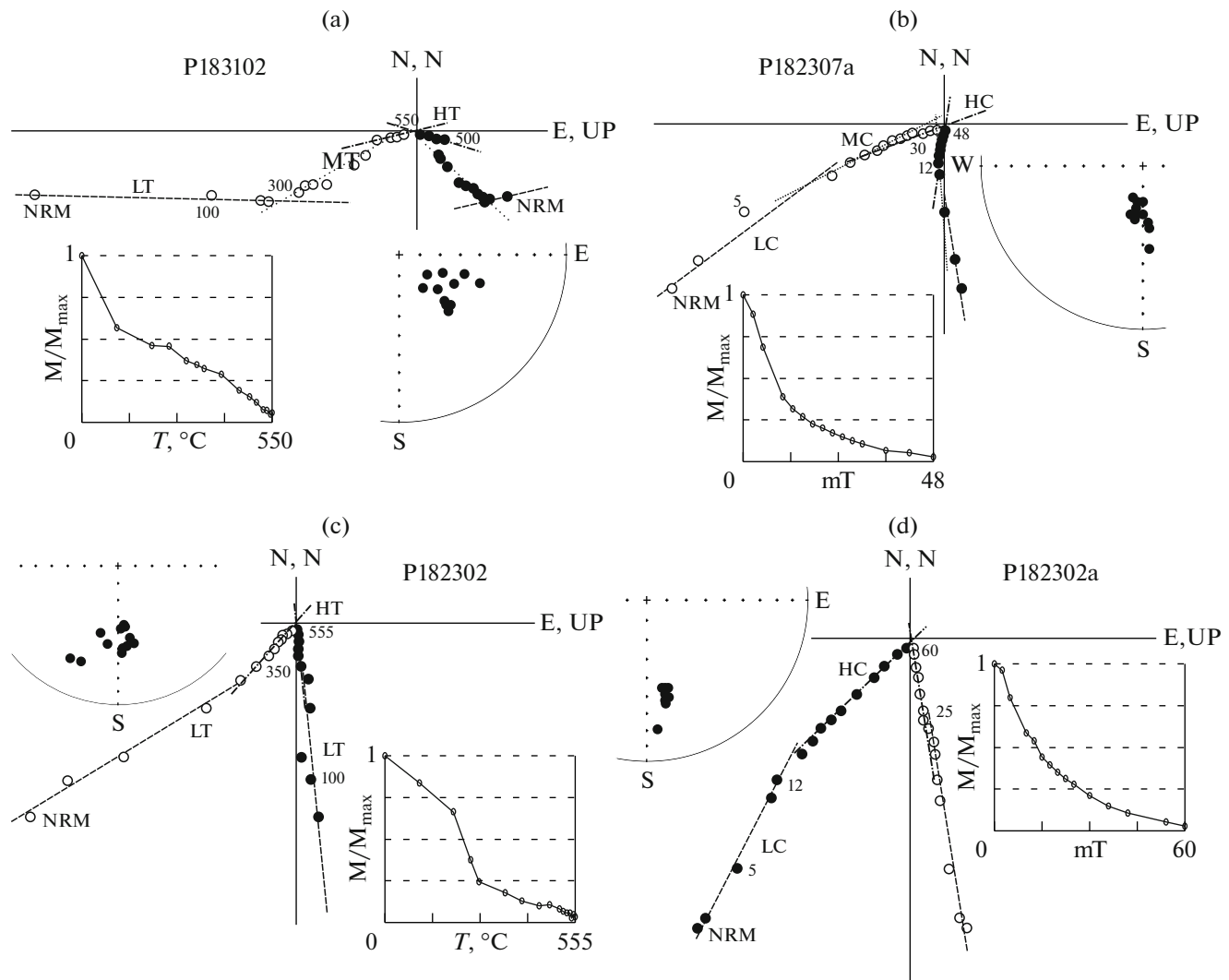


Fig. 5. Examples of the orthogonal demagnetization diagrams (in the geographical coordinate system) of the samples with two- (c, d) and three-component (a, b) NRM compositions determined from T - (a, c) and H -demagnetization procedures (b, d).

pling area: ($D = 0^\circ$, $I = 68^\circ$). We suggest that this behavior is due to the laboratory (viscous) NRM component that was acquired during the sample preparation. The deviation of the mean-site direction for the second group from the present day magnetic field direction may be linked to a significant effect of the viscous NRM component.

The MT and MC components of the NRM have not been analyzed for the studied samples, as they have only been identified in 10% of cases and do not show a stable direction.

The HC and HT components of the NRM show similar directions (Fig. 6, Table 1), which supports the primary origin of this component. The orthogonal demagnetization diagrams plotted using the H - and T -demagnetization results obtained for all samples clearly show the HC and HT components of the NRM in the ranges between 25–60 mT and 430–570°C,

respectively, that coincide at the starting coordinate point, as a rule. To conclude, this component may be considered as the ChRM component for Middle Jurassic sandstones of the Elgon Formation of the Ulban Terrane. Using the ChRM component, we have calculated the paleomagnetic pole coordinates and the paleolatitude at which these rocks were deposited: $Plat = -34.3$ (34.3°); $Plong = 161.2$ (341.2°); $dm = 2.7$, $dp = 5.3$, the paleolatitude = 0.1° ($+2.7^\circ/-2.6^\circ$) S longitude (see Table 1).

Fold test. The ChRM component has been recognized in 106 samples from the total of 144 samples. In the stratigraphic coordinate system we observed an increase in the grouping of the distribution of this component, namely, by a factor of 1.7 for the samples, and more than two times for the sites: $Ks/Kg = 2.26$ (Table 1) The maximum grouping was observed when the 80% correction was introduced for the bed strike

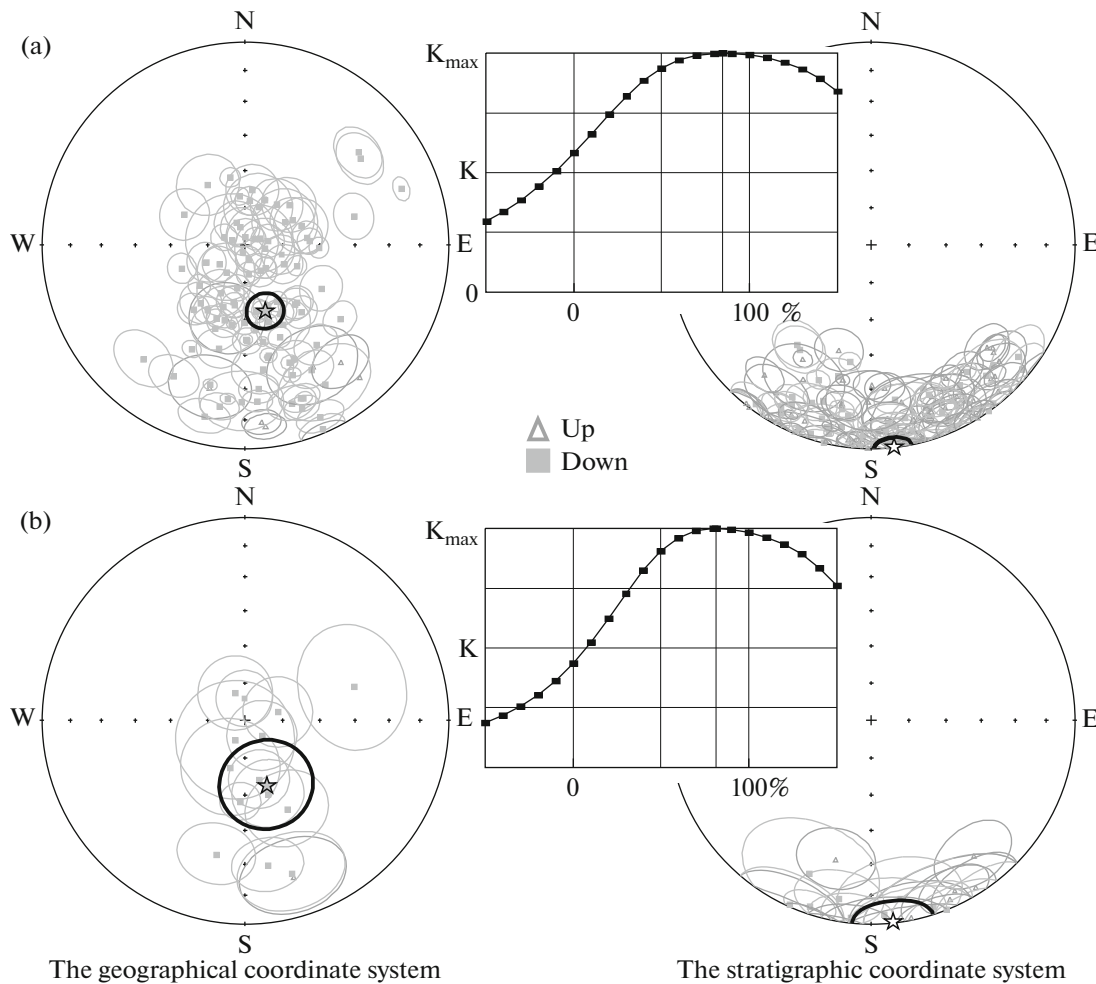


Fig. 6. The distribution of projected ChRM directions in the sandstones of the Elgon Formation, for samples (a) and sampling sites (b). On the left, the geographical coordinate system; on the right, the stratigraphic coordinate system. The middle diagram depicts the fold test (the dependence of grouping of the ChRM distribution on the unfolding value, %). Asterisks show the ChRM mean directions.

and dip angles (Fig. 6), which is evidence of the pre-folding age of the ChRM, close to the time when these rocks were deposited.

The determination of the probable inclination shallowing. Sandstones were the focus of our study, as mentioned. The effect of the inclination shallowing of magnetization is typical of sedimentary rocks, which, in turn, affects the correctness of the results of paleomagnetic studies. This phenomenon was discovered experimentally by E. Johnson in the middle of the last century, when the NRM declination (Dec) value was found to be consistent with that of the Earth's magnetic field during the re-deposition of clays, whereas the NRM inclination (Inc) value appeared to be lower than that of the Earth's magnetic field. [28]. The effect may be insufficiently displayed and may lie within the paleomagnetic determination error (0° – 5°); however, it may attain a few tens of degrees, which considerably affects the calculations of the paleolatitudes at which

the rocks are deposited, and the paleomagnetic pole coordinate calculations [28, 33]. On this assumption, it seems reasonable to perform the calculations of the probable value of the ChRM inclination shallowing for the studied rocks. Given that the number of the analyzed samples (N) is over 100 and that the anisotropy coefficient of the initial magnetic susceptibility (P) is known for each sample, two independent methods may be involved to calculate the inclination shallowing value.

The details of the first method can be found in [31]. We employed this method to determine the ChRM inclination shallowing value in various rocks of the SAOB [1, 25]. The method is reduced to the calculation of the correlation coefficient (r_k) between the inverse anisotropy value of the initial magnetic susceptibility and the tangent of the ChRM inclination angle. The calculations did not reveal a relationship between these two parameters ($r_k \sim -0.1$), which indi-

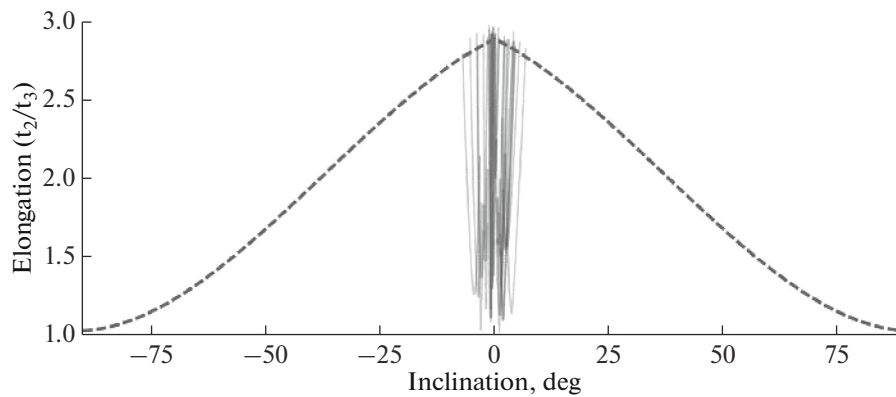


Fig. 7. Estimation of the inclination shallowing in the sandstones of the Elgon Formation using the E–I method. Dashed line, the expected E/I ratio, solid lines, the calculated values of the E/I ratios, obtained by modeling.

icates the lack of the inclination shallowing effect in the studied rocks.

The second method, “Elongation–Inclination” (E–I) [38, 39], rests on the calculation of the inclination shallowing coefficient f using the statistical method in [33]. To apply this method, we required a sampling of no less than 80–100 samples; in our case, this condition is satisfied. Successful practical examples that illustrate the application of this method have been given in many publications, for instance, [27]. A good convergence between the calculation results obtained using the E–I method and the experimental data on the re-deposition of the sedimentary rocks is reported in [34]. Our calculations show that the inclination shallowing value is less than 1° (Fig. 7), which, first, lies within the determination error of the paleomagnetic method, and, second, points to the lack of the effect of significant inclination shallowing of the ChRM vector in the sandstones of the Elgon Formation.

DISCUSSION

The first point concerns the determination of the polarity of the obtained paleomagnetic pole. The available data are insufficient to solve this problem. This is the reason that an unequivocal solution of this problem is not possible. The obtained ChRM direction, which is close in time to the deposition of the rocks of the Elgon Formation ($Dec_g = 163.1^\circ$, $Inc_g = 62.2^\circ$), may possess both direct and reversed polarities. However, we assume that this is not fundamental for the solution of the magnetotectonic problem, which is the goal of our study, since the obtained paleolatitude values are close to the equatorial ones. The problem of polarity determination may be solved by involving new paleomagnetic data on other objects of the Ulban Terrane.

The second part of the discussion considers the interpretation of the obtained paleolatitudes at which

the sandstones of the Elgon Formation of the Ulban Terrane were deposited. According to different authors [3, 17, 24, 29, 35, 36, and others], several models exist that describe the formation of the Mongol–Okhotsk Orogenic Belt, which mainly differ in the configuration and the time of the formation of the paleobasin. However, all these models rest on similar concepts on the paleolatitudes at which the Mongol–Okhotsk paleobasin was located, which range from 40° N to 60° N. Conversely, lower paleolatitudes are typical of the terranes that are included in the Sikhote Alin Orogenic Belt and the adjacent Sakhalin Branch; these paleolatitudes vary between 0 – 5° N and 35 – 50° N [1, 8, 11, 12, 15, 25, 30]. As a rule, the rocks of older terranes of the SAOB are found to have been deposited at lower latitudes (Fig. 8).

The paleomagnetic data on Middle Jurassic sandstones of the Elgon Formation of the Ulban Terrane support their being part of the SAOB, because the paleolatitudes at which these rocks were deposited are close to the equatorial ones (Fig. 8). We may assume that the sedimentary rocks that were deposited in the Middle Jurassic turbidite basin at the boundary between the Asian paleocontinent and the Paleo Pacific were further translated northward along the “continent–ocean” boundary for more than 5000 km.

We adduce one more argument in favor of the attribution of the Ulban Terrane to the structure of the Mongol–Okhotsk Fold Belt. According to new geochronological and geological-structural data reported by Sorokin et al. [37] the lack of detrital zircons that were dated earlier than 171 Ma in the sedimentary rocks of the eastern link of the Mongol–Okhotsk basin supports its complete closure at the Early-to-Middle Jurassic boundary.

It should be noted that the inferred equatorial paleolatitudes at which Middle Jurassic rocks of the Elgon Formation were deposited are not consistent with the findings of the boreal fossil fauna in the Jurassic deposits of the Ulban Terrane [2]. To resolve this

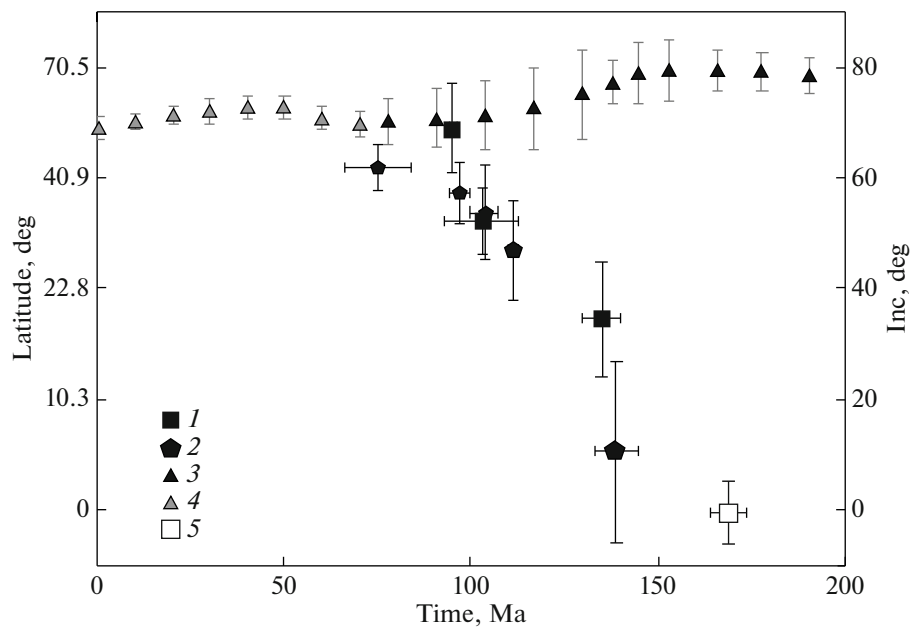


Fig. 8. Comparison between the paleolatitudes at which Middle Jurassic sedimentary rocks of the Elgon Formation of the Ulban Terrane were deposited, and the paleolatitude locations of the Sikhote Alin—North Sakhalin Orogenic Belt and the Eurasian continent for the time period of 0–200 Ma. (1, 2) Paleolatitudes at which the rocks of the Sikhote Alin—North Sakhalin Orogenic Belt were formed: (1) after [14]; (2) after [30]; (3, 4) the paleolatitude of the Eurasian continent: (3) after [13]; (4) after [40]; (5) the paleolatitude at which Middle Jurassic sedimentary rocks of the Elgon Formation of the Ulban Terrane were deposited (the present paper).

contradiction, we need to conduct further studies. It is worth noting that according to [2], ammonites of the *Harpoceras* and *Pseudolicerias* genera have only been identified in the Mikhailitsinsky Formation of the Amgun River basin, while retroceramuses have been found in the same basin, but in the Elgon Formation. Belemnite fragments (a few examples) and picea and pollen have only been detected in the coastal outcrops along the Ulban Bay for which the paleomagnetic data were obtained. Findings of *Bennettites*, which, according to [23], preferred a warm climate without seasonal temperature variations, have been discovered among the latter.

CONCLUSIONS

These studies have shown that most of the samples have a two-component NRM composition; the HT and HC components of their NRM appear to be pre-folding and are considered as the ChRM components for Middle Jurassic sandstones of the Elgon Formation of the Ulban Terrane. Based on these data, the following inferences can be made:

(1) The sedimentary rocks of the Ulban Terrane were deposited at near-equatorial paleolatitudes;

(2) In the post-Middle Jurassic, the rocks of the Elgon Formation drifted northward along the “continent–ocean” boundary for more than 5000 km up to their present day location;

(3) The Ulban Terrane is integrated in the system of the Sikhote Alin Orogenic Belt, which is consistent with the concept proposed by Golozubov [7].

ACKNOWLEDGMENTS

The authors express their sincere gratitude to the reviewers V.Yu. Vodovozov and V.V. Golozubov whose useful remarks and suggestions improved the quality of the manuscript. Thanks are also due to S.V. Burya, E.Yu. Didenko, and O.M. Menshikova for technical support during the fieldwork and the manuscript preparation.

FUNDING

The studies were supported by the RFBR within the framework of research projects nos. 21-55-50001 and 18-35-00048.

REFERENCES

1. M. V. Arkhipov, I. P. Voinova, A. V. Kudymov, A. Yu. Peskov, Sh. Oto, M. Nagata, V. V. Golozubov, and A. N. Didenko, “Comparative analysis of Aptian–Albian Rocks of the Kema and Kiselevka–Manoma terranes: geochemistry, geochronology, and paleomagnetism,” *Russ. J. Pac. Geol.* **13** (3), 239–264 (2019).
2. M. A. Akhmet’ev, V. B. Karaulov, A. A. Kozlov, E. D. Konyushkov, Yu. I. Potapov, G. I. Kharitonychev, and V. A. Shurshalina, “New data on stratigraphy

- of the Jurassic deposits of the Northern Amur Region,” *Sov. Geologiya*, No. 8, 112–119 (1967).
3. *Geodynamics, Magmatism, and Metallogeny of East Russia*, Ed. by A.I. Khanchuk (Dal’nauka, Vladivostok, 2006) [in Russian].
 4. *Geological Map of the USSR. 1 : 200000. Lower Amur Series. Sheet N-54-XIX: Explanatory Note*, Ed. by E.D. Konyushkov, V.A. Mikhal’tsev, S.V. Beletskaya (VGF, Moscow, 1974), p. 91 [in Russian].
 5. *Geological Map of the USSR. 1 : 200000. Uda Series. Sheet N-53-XXIV: Explanatory Note*, Ed. by G. I. Kharitonoychev, V. V. Vikhlyantsev, A. I. Savchenko (VANPO “Aerogeologiya”, Moscow, 1978) [in Russian].
 6. V. V. Golozubov, *Extended Abstract of Candidate’s Dissertation in Geology and Mineralogy* (Moscow, 2004) [in Russian].
 7. V. V. Golozubov, *Tectonics of the Jurassic and Lower Cretaceous Complexes of the Northwestern Margin of the Pacific Ocean* (Dal’nauka, Vladivostok, 2006) [in Russian].
 8. V. V. Golozubov, A. I. Malinovsky, and V. P. Simanenko, “Tectonic reconstruction of the Sikhote-Alin chain of the East Asian Margin: are simple solutions possible?,” *Tikhookean. Geol.* **25** (4), 115–119 (2006).
 9. *State Geological Map of the Russian Federation 1 : 1000000. Sheet N-53 (3rd Generation). Far East Series. Explanatory Notes* Ed. by V. Yu. Zabrodin, V. A. Gur’yanov, S. G. Kislyakov (VSEGEI, St. Petersburg, 2007), p. 448 [in Russian].
 10. R. Gradzinskii, A. Kostetskaya, A. Rodomskii, and R. Ungur, *Sedimentology* (Nedra, Moscow, 1980) [in Russian].
 11. A. N. Didenko, A. I. Khanchuk, A. I. Tikhomirova, and I. P. Voinova, “Eastern segment of the Kiselevka–Manoma Terrane (Northern Sikhote Alin): paleomagnetism and geodynamic implications,” *Russ. J. Pac. Geol.* **8** (1), 18–37 (2014).
 12. A. N. Didenko, A. I. Khanchuk, and A. I. Tikhomirova, “Paleomagnetism of the Kiselevka Complex of the Kiselevka–Manoma Terrain (Sikhote-Alin): geodynamic consequences,” *Dokl. Earth Sci.* **454** (2), 108–113 (2014).
 13. A. N. Didenko, “The analysis of Meso–Cenozoic paleomagnetic poles and the apparent polar wander path of Siberia,” *Izv., Phys. Solid Earth* **51** (5), 674–688 (2015).
 14. A. N. Didenko, A. Yu. Peskov, A. V. Kudymov, I. P. Voinova, A. I. Tikhomirova, and M. V. Arkhipov, “Paleomagnetism and accretionary tectonics of northern Sikhote Alin,” *Izv., Phys. Solid Earth* **53** (5), 733–749 (2017).
 15. A. N. Didenko and A. I. Khanchuk, “Change in the geodynamic settings in the Pacific–Eurasia transition zone at the end of the Early Cretaceous,” *Dokl. Earth Sci.* **487** (2), 873–876 (2019).
 16. L. P. Zonenshain, M. I. Kuzmin, and V. M. Moralev, *Global Tectonics, Magmatism and Metallogeny* (Nedra, Moscow, 1976) [in Russian].
 17. Zonenshain, L.P., Kuzmin, M.I., and Natapov, L.M., *Plate Tectonics of the USSR Territory* (Nauka, Moscow, 1990) [in Russian].
 18. S. V. Zyabrev and E. K. Shevelev, “Accretion of the Anuy Zone, tectonic zonation, and evolution of the Samarka Accretionary Complex: details of evolutionary scenario of the Sikhote-Alin Segment of the East Asian continental margin,” *Russ. J. Pac. Geol.* **13** (6), 535–555 (2019).
 19. A. A. Maiboroda and L. I. Sharueva, “Formational affiliation and composition of the Jurassic sediments of the western Ul’ban foredeep (Okhtsk region),” in *Sedimentary and Volcanogenic–Sedimentary Formations of the Far East* (DVNTs AN SSSR, Vladivostok, 1979), pp. 27–36 [in Russian].
 20. D. V. Metelkin and A. Yu. Kazanskii, *Principles of Magnetotectonics. A Textbook* (Novosib. Gos. Univ., Novosibirsk, 2014) [in Russian].
 21. M. S. Nagibina, *Tectonics and Magmatism of the Mongol–Okhotsk Belt* (Izd-vo AN SSSR, Moscow, 1963) [in Russian].
 22. B. A. Natal’in and Ch. B. Borukaev, “Mesozoic structures of the southern Soviet Far East,” *Geotektonika*, No. 1, 84–96 (1991).
 23. *Principles of Paleontology. A Reference Book for Paleontologists and Geologists of the USSR. Gymnosperms and Angiosperms*, Ed. by A. L. Takhtadzhyan, V. A. Vakhrameev, and G. P. Radchenko (Gos. Nauchn.-Tekhn. Izd. Literaturny Geol. Okhr. Nedr, Moscow, 1963) [in Russian].
 24. L. M. Parfenov, N. A. Berzin, A. I. Khanchuk, G. Bardarch, V. G. Belichenko, A. N. Bulgatov, S. I. Dril’, G. L. Kirillova, M. I. Kuz’min, U. Nokleberg, A. V. Prokop’ev, V. F. Timofeev, O. Tomurtogoo, and H. Jahn, “Model of formation of orogenic belts of the Central and Northeastern Asia,” *Tikhookean. Geol.* **22** (6), 7–41 (2003).
 25. A. Yu. Peskov, A. N. Didenko, A. V. Kudymov, A. S. Karetnikov, M. V. Arkhipov, “Paleomagnetism and petrochemistry of sandstones from the Gorinskaya and Pionerskaya formations, Zhuravlevka–Amurian Terrane (Northern Sikhote Alin),” *Russ. J. Pac. Geol.* **13** (6), 556–567 (2019).
 26. D. M. Pecherskii and A. N. Didenko, *Paleozoic Ocean: Petro-magnetic and Paleomagnetic Information on Its Lithosphere* (OIFZ RAN, Moscow, 1995) [in Russian].
 27. A. M. Fetisova, R. V. Veselovskiy, F. Scholze, and Yu. P. Balabanov, “The new Permian–Triassic paleomagnetic pole for the East European Platform corrected for inclination shallowing,” *Izv., Phys. Solid Earth* **54** (1), 150–162 (2018).
 28. A. N. Khramov, G. I. Goncharov, R. A. Komissarova, V. V. Pisarevskii, and E. M. Gurevich, *Paleomagnetology* (Nedra, Leningrad, 1982) [in Russian].
 29. B. F. Shevchenko, L. I. Popeko, and A. N. Didenko, “Tectonics and evolution of the lithosphere of the Eastern fragment of the Mongol–Okhotsk orogenic belt,” *Geodynam. Tectonophys.* **5** (3), 667–682 (2014).
 30. A. Abrajevitch, K. Kodama, S. Zyabrev, and A. N. Didenko, “Palaeomagnetism of the West Sakhalin Basin: evidence for northward displacement during the Cretaceous,” *Geophys. J. Int.* **190** (3), 1439–1454 (2012).
 31. N. Bradbury, “Correcting for Paleomagnetic Inclination Shallowing in Magnetite-Bearing Clay-Rich Soft Sediments with the Aid of Magnetic Anisotropy and

- Uniaxial Compression Experiments,” *Thesis Master of Science* (St. John’s, Newfoundland, 2005).
32. R. J. Enkin, “A computer program package for analysis and presentation of paleomagnetic data,” Pacific Geosci. Centre, Geol. Surv. Canada, 16 (1994).
 33. R. F. King, “The remanent magnetism of artificially deposited sediment,” *Geophys. J. Int.* **7** (Suppl. 3), 115–134 (2007).
 34. K. Kodama, *Paleomagnetism of Sedimentary Rocks: Process and Interpretation* (Wiley-Blackwell, 2012).
 35. A. Kroner, V. P. Kovach, I. Kozakov, T. Kirnozova P. Azimov, J. Wong, and H. Y. Geng, “Zircon ages and Nd–Hf isotopes in UHT granulites of the Ider Complex: a cratonic terrane within the Central Asian Orogenic Belt in NW Mongolia,” *Gondwana Res.* **27** (4), 1392–1406 (2015).
 36. S. Maruyama, Y. Isozak, G. Kimura, and M. Terabayashi, “Paleogeographic maps of the Japanese islands: plate tectonics synthesis,” *Island Arc* **6** (1), 121–142 (1997).
 37. A. A. Sorokin, A. A. Zaika, V. P. Kovach, A. B. Kotov, C. Xu Wenliang, and Hao Yang, “Timing of closure of the Eastern Mongol–Okhotsk Ocean: constraints from U–Pb and Hf isotopic data of detrital zircons from metasediments along the Dzhagdy Transect,” *Gondwana Res.* **81**, 58–78 (2020).
 38. L. Tauxe and D. V. Kent, “A simplified statistical model for the geomagnetic field and the detection of shallow bias in paleomagnetic inclinations: was the ancient magnetic field dipolar?,” *Timescales of the Paleomagnetic Field* (Am. Geophys. Union, Washington, DC, 2004), Vol. 145, pp. 101–116.
 39. L. Tauxe, K. Kodama, and D. V. Kent, “Testing corrections for paleomagnetic inclination error in sedimentary rocks: a comparative approach,” *Phys. Earth Planet. Int.* **169**, 152–165 (2008).
 40. T. H. Torsvik, R. D. Muller, R. Van der Voo, B. Steinberg, and C. Gaina, “Global plate motion frames: toward a unified model,” *Rev. Geophys.* **46** (3), RG3004 (2008).
 41. J. D. A. Zijderveld, A.C. demagnetization of rocks: analysis of results,” *Methods in Paleomagnetism*, Ed. by D. W. Collinson and K. M. Creer (Elsevier, Amsterdam, 1967), pp. 254–286.

Recommended for publishing by V.V. Golozubov
Translated by N. Kovriga